

See discussions, stats, and author profiles for this publication at: <https://www.researchgate.net/publication/273835553>

DFT-Aided Vibrational Circular Dichroism Spectroscopy Study of (–)-S-cotinine

ARTICLE *in* CHEMPHYSCHM · MARCH 2015

Impact Factor: 3.42 · DOI: [10.1002/cphc.201500018](https://doi.org/10.1002/cphc.201500018)

CITATION

1

READS

85

4 AUTHORS, INCLUDING:



F. Márquez

Universidad de Jaén

32 PUBLICATIONS 228 CITATIONS

[SEE PROFILE](#)



J. J. López González

Universidad de Jaén

134 PUBLICATIONS 1,138 CITATIONS

[SEE PROFILE](#)

DFT-Aided Vibrational Circular Dichroism Spectroscopy Study of (–)-S-cotinine

Pilar G. Rodríguez Ortega, Manuel Montejo,* Fernando Márquez, and Juan J. López González^[a]

The implementation of a strategy comprising the use of vibrational circular dichroism spectroscopy and DFT calculations allows determination of the solution-state conformational distribution in (–)-S-cotinine, giving further proof of the extra conformer-discriminating potential of this experimental technique, which may offer unique molecular fingerprints of subtly dissimilar molecular conformers of chiral samples. Natural

bond orbital electronic structure calculations of the rotational barrier height between the two main conformers of the species indicate that hyperconjugative effects are the key force governing the conformational equilibrium. The negligible effect of the solvent's polarity over both structure and conformational energy profile supports this result.

1. Introduction

The term alkaloid is applied to stand for alkaline heterocyclic compounds with one or more nitrogen atoms in their structure that are derived from plant sources (i.e. occurring naturally) and that usually have a marked physiological role.^[1] Although little convincing evidence for their function has been achieved so far, due to their highly diverse natures, they have been suggested to play extremely diverse roles such as: storing or transporting (in soluble form) particularly needed acids, plant metabolism, plant defence against singlet oxygen ($^1\text{O}_2$), and plant defence against other aggressors.

Nicotinoids constitute a group of alkaloids whose structures have in common a two-ring assembly with a 3-pyridyl methylamine skeleton. The structural prototype of the nicotinoids is nicotine (the major alkaloid in tobacco leaves), namely, 1-methyl-2-(3-pyridyl)pyrrolidine. This system has been deeply investigated mainly in relation with its role as agonist of the acetylcholine receptor (nAChR).^[2,3]

The search of new agonists of nAChR is an active field of research owing to the fact that they can be used for the treatment of numerous diseases such as Alzheimer's and Parkinson's diseases, Tourette's syndrome, schizophrenia, anxiety, cognitive and attention deficits, and tobacco addiction.^[4–8]

Two pharmacophores have been identified in nAChR: 1) one lone electron pair (the agonist–AChR interaction occurs through hydrogen bonding) and 2) a positively charged nitrogen center (the π cloud of the agonist interacts with the cationic center in AChR).^[9–11] Given the potential utility of nicotinoids as nAChR's agonist, the conformational preference in nic-

otine and other structurally related species have been the subject of several studies, both theoretical and experimental.^[12–30]

(–)-S-cotinine (one of the minor alkaloid tobacco constituents) is the major peripheral oxidative metabolite of (–)-S-nicotine in several animal species, including humans, and has been shown to be the most abundant (–)-S-nicotine metabolite in the central nervous systems of rats after administration of nicotine.^[31,32] The fact that this metabolite does not undergo significant biotransformation in brain tissue *in vivo* and that it has much longer half-life in the central nervous system than does (–)-S-nicotine^[31,32] turn it into a very attractive molecular target for the design of new nicotinoidal structure-based agonists of nAChR. Indeed, the efficiency of (–)-S-cotinine for the treatment of Alzheimer's disease and Parkinson's disease due to its acceptable ability to bind to nACh receptors of the brain of patients while acting as a nicotinic agonist has already been described.^[33] Besides, (–)-S-cotinine stimulates nicotinic receptors to evoke the release of dopamine, meaning that (–)-S-cotinine likely contributes to the neuropharmacological effects of nicotine and tobacco use.^[32] Beyond that, (–)-S-cotinine have also yielded positive results in assisting tobacco withdrawal and in the treatment of psychiatric disorders such as obsessive-compulsive disorder, Tourette's syndrome and schizophrenia.^[33]

Since nicotinoid agonists' activity against nAChR depends on the intramolecular N–N distance,^[27] which is conditional on the molecular conformation adopted, getting insight into the molecular and electronic structure, conformational and electronic properties of (–)-S-cotinine can help to get a better understanding of the molecular recognition mechanisms in nAChR which, in turn, are very valuable for the elucidation of the nature and magnitude of their interactions with the molecular targets.

Despite the important biological role that this and other structurally related compounds may play, the number of studies focused on the structural characterization of (–)-S-cotinine

[a] P. G. Rodríguez Ortega, Prof. M. Montejo, Prof. F. Márquez,
Prof. J. J. López González
Department of Physical and Analytical Chemistry
University of Jaén, 23071 Jaén (Spain)
E-mail: mmontejo@ujaen.es

 Supporting Information for this article is available on the WWW under
<http://dx.doi.org/10.1002/cphc.201500018>.

is relatively scarce. Indeed, it has been the subject of several works mainly focused on its molecular structure and conformational distribution in the gas phase,^[25,34] its basicity equilibrium constants^[35] and its analytical determination.^[36,37] Nevertheless, the conformer distribution of the species in solution as well as the mechanisms controlling its conformational equilibrium (both in the gas phase and in solution) still remain unclear.

In this work, we present a thorough theoretical and experimental analysis of the conformational landscape, the rotational isomerism barrier and solution-state conformational energy profile of (–)-S-cotinine. For this task, we have taken advantage of the known hypersensitivity of the vibrational circular dichroism (VCD) technique towards the three-dimensional structure of chiral compounds (both pure and in solution). In fact, we report here the first records, to the best of our knowledge, of the VCD spectra of (–)-S-cotinine (in pure-phase and in CCl₄ solution).

Our approach consists of a thorough in silico conformational search (performed using MM, ab initio and DFT calculations) and a detailed vibrational analysis of the VCD and FTIR spectra of the species, which allows validating our theoretical models and confirms the occurrence of conformational mixture in the sample. Further, we have implemented the natural bond orbitals (NBO) method in order to get a better understanding of the conformational change mechanisms and associated barriers heights, as well as to judge the extension in which these are influenced by electrostatic (including the role of solvents of different polarities) and/or hyperconjugative effects. It is worth to mention that, in case the conformational preference of (–)-S-cotinine would be controlled by hyperconjugative mechanisms, the polarity of the surrounding medium should not largely affect the conformational distribution of the species, which would allow a tentative extrapolation of our results to the behavior of the system in water (leaving aside auto-ionization processes), a solvent that may blur the interpretation of the VCD spectra.

Computational Methods

A conformational search for (–)-S-cotinine was performed by MM calculations using the MMFF^[38–42] and SYBYL^[43] force fields as implemented in SPARTAN08 program package^[44] and employing the Monte Carlo methodology.

Geometrical optimizations (with ab initio and DFT methods) of the selected non-redundant minimum energy conformers and the computation of their harmonic vibrational wavenumbers were performed using the Gaussian 09 (Revision D.01) suite of programs.^[45] Geometry optimization criteria were those corresponding to SCF=Tight and Int=Ultrafine. Becke's three-parametric hybrid exchange functional^[46] combined with the Lee-Yang-Parr correlation functional^[47] and with the exchange component of Perdew and Wang's 1991 functional^[48–50] (i.e., the B3LYP and B3PW91 hybrid functionals) were used in conjunction with the 6-311+ +G**^[51] and aug-cc-pVTZ^[52] basis sets. In order to validate minima and structures, the MP2 method^[53] in conjunction with the 6-31+G* basis set^[54,55] were also used. Solvent effects were taken into account by applying the integral equation formalism version of the polarizable continuum solvation model (IEF-PCM method^[56–60]) using the dielectric constants corresponding to CCl₄ ($\epsilon=2.2$) and DMSO ($\epsilon=46.8$) and

with a cavity build up using UFF radii (explicit treatment for hydrogens) as implemented in Gaussian 09.

All simulated spectra have been broadened by a Lorentzian function with a full-width at half-maximum (FWHM) of 8 cm^{–1}. Finally, natural bond orbital (NBO)^[61] calculations were accomplished using the program NBO v.6.0.^[62]

Experimental Procedure, Materials and Methods

Commercial (–)-S-cotinine was purchased from Alfa-Aesar and used without further purification.

The mid-IR and VCD spectra of the sample were recorded in solid phase (Nujol mulls) and in solution (CCl₄) using a JASCO FVS-4000 FTIR spectrometer, equipped with InSb (4000–1900 cm^{–1}) and MCT (2000–900 cm^{–1}) detectors, standard liquid cells and BaF₂ windows. The spectra in the 2000–900 cm^{–1} range were acquired using a spectral resolution of 4 cm^{–1} and 8000 scans (in blocks of 2000 scans; Nujol mulls) and 2000 scans (CCl₄ solutions).

The measurement of the VCD spectra of solid (–)-S-cotinine was performed so as to avoid the main artifacts sources when recording VCD spectra of solid samples: scattering effects related to particle size and linear birefringence.^[63] For that, very small quantities (a few milligrams) of the sample were deeply disaggregated in Nujol in order to get suitable mulls. Avoiding the presence of linear birefringence artifacts was ensured by rotating the sample cell about the light propagation axis, both parallel (90°, 180° and 270°) and perpendicular to it.^[64]

The concentration ranges of the CCl₄ solutions were optimized to get the optimum absorbance range for the VCD and IR measurements. Hence, solutions with concentrations ranging from 0.5 M to 2 M and cell path-lengths of ca. 5–50 μm were employed as recommended elsewhere.^[65,66] Specifically, for the 2000–1600 cm^{–1} spectral range we report the spectra obtained using concentrations of 0.1–0.2 M and 25 μm cell path-lengths, whilst for the 1600–900 cm^{–1} region the reported spectra were obtained using concentrations ranging from 1 M to 2 M along with 50 μm cell path-lengths. In this way, the IR absorbance achieved always suitably lay in the range 0.12–0.9.^[63]

Baseline corrections were performed by subtracting the raw VCD spectra of pure Nujol and CCl₄ from the VCD spectra of the samples in solid phase and in solution, respectively.

2. Results and Discussion

2.1. Conformational Analysis and Molecular Structure of (–)-S-cotinine

Because the vibrational spectrum profiles arise from the combined contribution of all the possible populated molecular conformations adopted by the sample at the experiment's conditions, a good match between theory and experiment (and, hence, the validation of the conclusions deduced) is unreachable unless a comprehensive study of the conformational landscape for the target molecule had been performed.

Figure 1 shows a schematic representation of the set of conformers expected for (–)-S-cotinine according with the main flexibility sources in its molecular structure (see Figure 2 for atom numbering). The pyrrolidinone ring in (–)-S-cotinine can adopt two non-equivalent envelope forms, namely envelopes 1 and 2 (Figure 1), which are the pyridine ring oriented in equa-

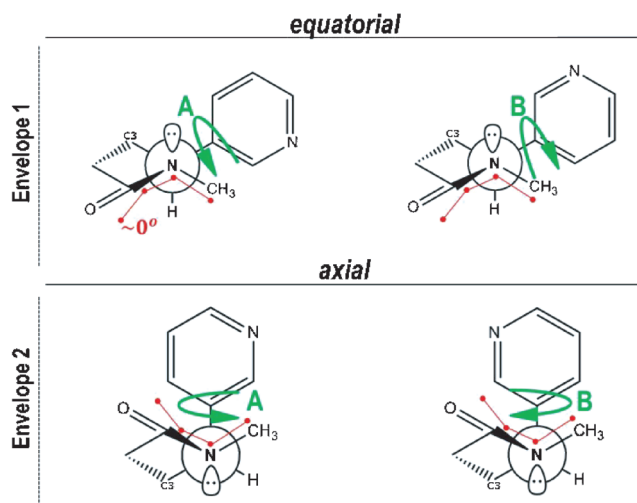


Figure 1. Schematic representation of the set of conformers of $(-)$ -S-cotinine taken into account for the DFT conformational search.

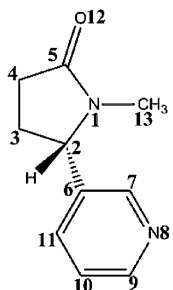


Figure 2. Atom numbering employed for $(-)$ -S-cotinine in the present study.

atorial and axial positions, respectively. For each of these conformations there is another degree of freedom related to the internal rotation of the C–C bond connecting the two rings, which generates two additional rotational isomers, so that the conformational variety of $(-)$ -S-cotinine is spread up to four structures. Therefore, our initial set of structures consisted of four designed conformations, which were subsequently optimized at a moderate level of theory (B3LYP/6-31+G^{*}). The absence of imaginary frequencies in their calculated harmonic vibrational spectra confirmed them as real minima on the potential energy surface. The consistency of our conformational search was further corroborated by an additional molecular-mechanics-based search (MMFF and SYBYL) that lead to no other than those four conformers already characterized as minima by the DFT calculations.

2.2. Gas-Phase Structure of $(-)$ -S-cotinine

Theoretical geometries for the set of conformers in the gas phase are in agreement with those determined experimentally using gas electron diffraction.^[34] The main structural differences within the whole set of conformers are the values of the dihedral angles C3–C2–C6–C7 (related to the internal rotation of the pyridine ring respect to the saturated heterocycle) and

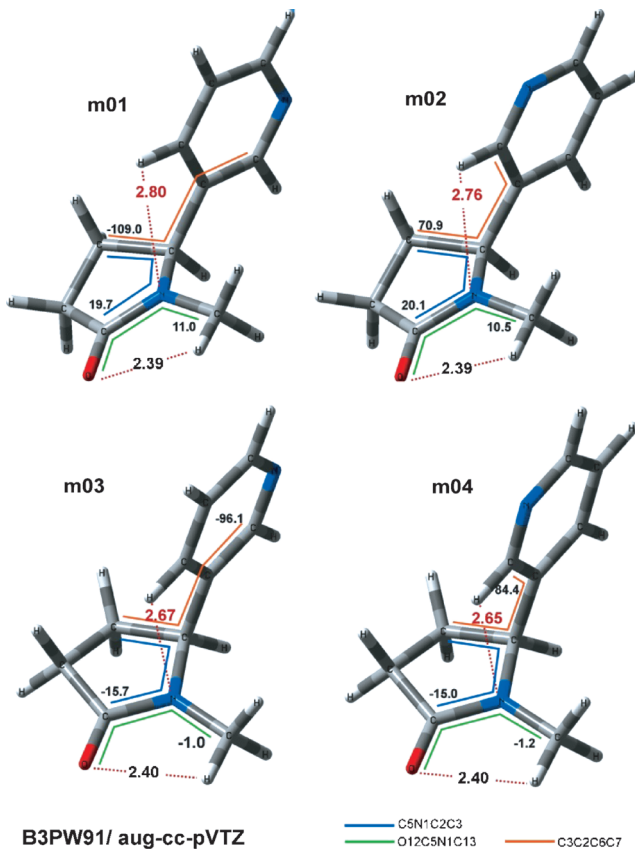


Figure 3. Optimized structures of conformers for $(-)$ -S-cotinine molecule at the B3PW91/aug-cc-pVTZ level of theory.

C5–N1–C2–C3 (which account for the puckering of the pyrrolidine ring) as shown in Figure 3. The value of the C3–C2–C6–C7 dihedral angle is in the -95° to -110° range for conformers with orientation A of the pyridine ring and within the 70 – 85° range for conformers adopting orientation B (Figure 1). Ring strain in this set of conformers is compensated by the position of the C3 atom (see Figure 1), which is positioned out of the amide plane by $+20.0^\circ$ (**m01** and **m02**) and -15.0° (**m03** and **m04**). The dihedral angle involving the amide group (i.e., O12–C5–N1–C13) is close to 0° in all cases, indicating the coplanarity for those atoms.

Calculated relative energies (ΔG) and gas-phase Boltzmann populations (in percentage) are collected in Table 1. Energy profiles and relative populations obtained with the two implemented theoretical methods are comparable and both suggest that the four structures are energetically reachable and would be populated in the gas phase at room temperature. Our theoretical calculations point to the higher stability of conformer **m01** (which accounts for ca. 45% of the total sample composition) in the gas phase. Both methods agree that **m04** is the higher-energy conformer, with its theoretical contribution being at approximately 10%. Conformers **m02** and **m03** are very close in energy and they contribute to the total sample composition almost to the same extent (ca. 20% and 25%, respectively). These results are in agreement with those reported in Ref. [34] [%Pop. gas electron diffraction (GED) (460 K): 34% **m01**, 21% **m02**, 28% **m03** and 17% **m04**].

Table 1. Relative energies (ΔG in Kcal mol^{-1}) and Boltzmann's populations (%) calculated in the gas phase, and in CCl_4 and DMSO solutions (IEF-PCM) at 298.15 K for the (–)-S-cotinine set of conformers.^[a]

	B3LYP/aug-cc-pVTZ ΔG	B3PW91/aug-cc-pVTZ ΔG	Gas phase %Pop.	
m01	0.00	43.28	0.00	45.37
m02	0.45	20.21	0.47	20.59
m03	0.30	25.95	0.37	24.13
m04	0.84	10.56	0.90	9.90
CCl_4				
m01	0.00	45.83	0.00	45.03
m02	0.48	20.49	0.49	19.71
m03	0.43	22.00	0.37	24.10
m04	0.81	11.69	0.83	11.16
DMSO				
m01	0.00	36.53	0.00	39.50
m02	0.26	23.71	0.27	25.21
m03	0.17	27.62	0.36	21.49
m04	0.65	12.13	0.62	13.80

[a] Theoretical population calculated using the Boltzmann equation and taking $T=298.15\text{ K}$.

Based on geometrical grounds, the authors of Ref. [34] also mention the possible occurrence of an intramolecular hydrogen bond (Hbi) linking the carbonyl group and the H atom of the N–CH₃ group. Supporting their proposal, the results of our NBO analyses (MP2/6-31+G*) suggest the incidence of a weak C=O12…H contact. The value of the total charge transfer interaction energy $E_{\text{tot}}^{(2)}$ that, in the NBO scheme, can be related to the strength of the interaction is calculated to lie in the 0.74–0.78 kcal mol^{-1} range for the four conformers studied.

Another plausible way of structural stabilization would be the establishment of an additional Hbi between the N1 atom and the closest H atom in the pyridine ring, as proposed in the literature^[20] to occur in a closely related system such as (–)-S-nicotine. Nonetheless, although in (–)-S-cotinine the N…H-C calculated distances fall within an adequate range for such interaction (Figure 3), our NBO analysis did not allow the detection of any electronic delocalization from the lone pair at N1 to the so-called antibonding orbital of the C–H bond.

2.3. Rotational Energy Barrier

We performed a relaxed scan (MP2/6-31+G*, 18 steps of 10° each) of the dihedral angle N1–C2–C6–C7 of which the rotation leads to the **m01**↔**TS**↔**m02** interconversion, and did a full NBO analysis for each generated structure during the scan. Figure 4 represents the electronic rotational energy curve (MP2/6-31+G*) of the conformational change of (–)-S-cotinine from **m01** towards **m02** along with its corresponding NBO, Lewis and non-Lewis energy curves.

The Lewis component was obtained by deleting all Rydberg and antibonding orbitals from the NBO basis set, hence giving the energy of the idealized Lewis structures. The non-Lewis component corresponds to the energy-lowering derived from all the possible donor–acceptor or hyperconjugative interactions within one given structure.

The electronic energy difference between the global (**m01**) and local (**m02**) minima in the MP2 curve is 0.6 kcal mol^{-1} , reaching a value of 7.85 kcal mol^{-1} at its corresponding barrier height. This energy barrier is comparable in magnitude to those reported before for other nicotinoid analogues such as nicotine^[20] and anabasine.^[67]

The calculation of the Lewis and non-Lewis contribution to the total NBO energy for **m01**, **m02** and the TS, gives the Lewis and non-Lewis rotational barriers (green and mauve lines respectively, Figure 4), the combination of which produces the ΔE^{NBO} barrier (red line in Figure 4) which, naturally, matches the MP2 barrier.

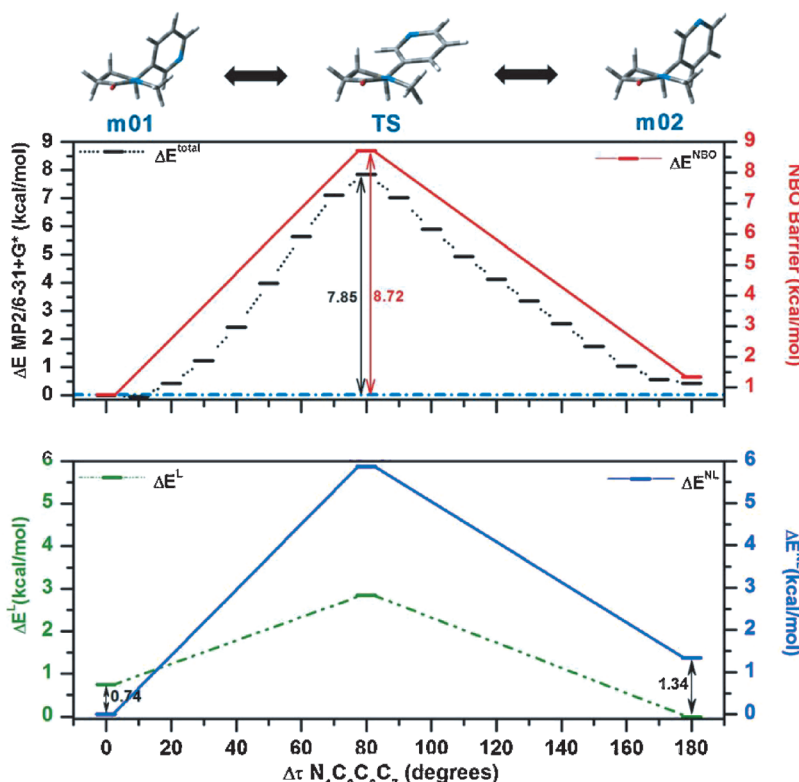


Figure 4. Energy curve for the **m01**↔**TS**↔**m02** rotational interconversion of (–)-S-cotinine calculated at the MP2/6-31+G* level (top, black curve), corresponding total NBO energy barrier (top, red line) and its Lewis (bottom, green line) and non-Lewis (bottom, mauve line) components.

The curves depicted in Figure 4 show that, while the energy associated with the Lewis structure of **m02** is 0.74 kcal mol⁻¹ lower than that for **m01**, stabilizing non-Lewis-type interactions are larger for **m01** (by 1.34 kcal mol⁻¹), tipping the conformational equilibrium balance towards **m01**, which is the global minimum. This suggests the dominant role of electronic delocalization and hyperconjugative effects in the conformational preference of this species. This behavior correlates with previous observations done for its chemical analogue, (–)-S-nicotine.^[30]

2.4. Structure in Solution

Theoretical relative energies and Boltzmann populations for the different conformers of (–)-S-cotinine in solution (CCl₄, $\epsilon = 2.2$; DMSO, $\epsilon = 46.8$) indicate that solvent's polarity does not noticeably alter the conformational energy profile since the relative energies hardly change when going from the gas phase to solution and neither do their theoretical populations.

Data reported in Table 1 show that, as in the gas phase, the **m01** structure is by far the most abundant conformer in both solvents, accounting for 45% (PCM-CCl₄, B3PW91/aug-cc-pVTZ) of the total sample composition. The other 55% is shared by the remaining conformers (**m02** ≈ 20%, **m03** ≈ 24% and **m04** ≈ 11%; the **m01:m02:m03:m04** ratio is close to 4:2:2:1). This is consistent with the fact that the conformational equilibrium in this species is controlled by hyperconjugation rather than electrostatic repulsions, as evidenced by NBO analysis. Nonetheless, a slight increase in the calculated amount of the less populated structures is observed in polar environments, that is, DMSO solution, possibly due to the minimization of intramolecular Lewis-type repulsive interactions on going from the gas phase to DMSO solution, but not enough to make these forms more stable than conformers **m01** and **m02** (*eq* structures) which are more stabilized by non-Lewis-type effects.

Similarity analyses performed for the theoretically determined molecular geometries in the gas phase, and in CCl₄ and DMSO solutions (IEF-PCM) also indicate the small effect that the surrounding medium has in the structure of (–)-S-cotinine conformers. The low root-mean-square (RMS) deviation values obtained account for this (see Figures S1 and S2, Supporting Information).

2.5. Vibrational Spectra and Experimental Conformational Population of (–)-S-cotinine

2.5.1. Solid-Phase and Solution-State IR and VCD Spectra and Theoretical Models

Figures 5 and 6 collect the recorded VCD and IR spectra for (–)-S-cotinine in solution (CCl₄) and in the solid phase (Nujol mull), respectively, in the 1800–900 cm⁻¹ spectral region. For the sake of clarity, all the experimental bands are marked and labeled numerically. Although we have also performed PCM calculations considering DMSO as solvent, the high polarity and presumably great tendency of DMSO to interact with solute molecules prevent us from using it in the experimental

measurement of the VCD spectrum of (–)-S-cotinine, since it is known that the use of highly polar media (i.e. interacting solvents) may lead to noticeable variations in the chiroptical responses of samples when recording VOA spectra.^[68] Besides, theoretical calculations predict slight solvent effects in calculated conformer populations and molecular geometries, hence presumably preventing the observation of differential features in the recorded spectra.

The differences that can be seen in both band shapes and relative intensities when comparing the VCD and IR spectral profiles of the sample in solution and the solid state are remarkable.

As known, the combined contribution of differently populated molecular conformations in solution contrasting the more limited and specific contributions of precise molecular conformations that may be present in a solid crystalline sample cause the vibrational bands in both solution-state IR and VCD spectra of a given species to be generally broader than their counterparts in solid-state spectra. However, we did observe a generalized band broadening in the solid-state spectra of (–)-S-cotinine that might be the result of crystal packing effects and/or intermolecular interactions, and could also be an indication of the occurrence of the Christiansen effect.^[69] This particle-size-related scattering effect usually produces a significant band-shape modification that may alter the vibrational profile of a solid-phase spectrum. Given the differential character of VCD spectroscopy, this effect may be especially noticeable in VCD spectra, hence leading to the obtaining of different phase-dependent spectral profiles.

Although we emphasize that we obtained several homogeneous mulls of highly disaggregated solid (–)-S-cotinine in Nujol, our analysis of the experimental data (Figures S4, S6, S8 and S10) does not allow us to discard the presence of particle-size-related scattering effects on the recorded VCD spectra.

Further, Boltzmann-weighted calculated spectra (using the implicit solvation model and considering the four conformers studied) allowed us to reach a good and reliable reproduction of the experimental features observed in the spectra recorded in CCl₄ (Figure 7 and Figures S3, S5, S7 and S9). Thus, for the abovementioned reasons, we take the spectra in solution as reference for the vibrational analysis.

As concerns the theoretical approximation, although we implemented B3PW91, which has been recommended for computing VCD intensities,^[70] we observed that in this case B3LYP (combined with the aug-cc-pVTZ basis set under the IEF-PCM model and using $\epsilon = 2.2$) performs similarly and even improves the description of the 1450–1350 cm⁻¹ region of the VCD spectrum (of key interest in this study). For that reason, we focus on B3LYP results.

2.5.2. Vibrational Assignment and Solution-State Conformer Populations

Table 2 collects the experimental wavenumbers of the VCD and IR bands marked in Figures 5 and 6, together with the theoretical vibrational wavenumbers calculated for the four conformers of (–)-S-cotinine (B3LYP/aug-cc-pVTZ), their associated

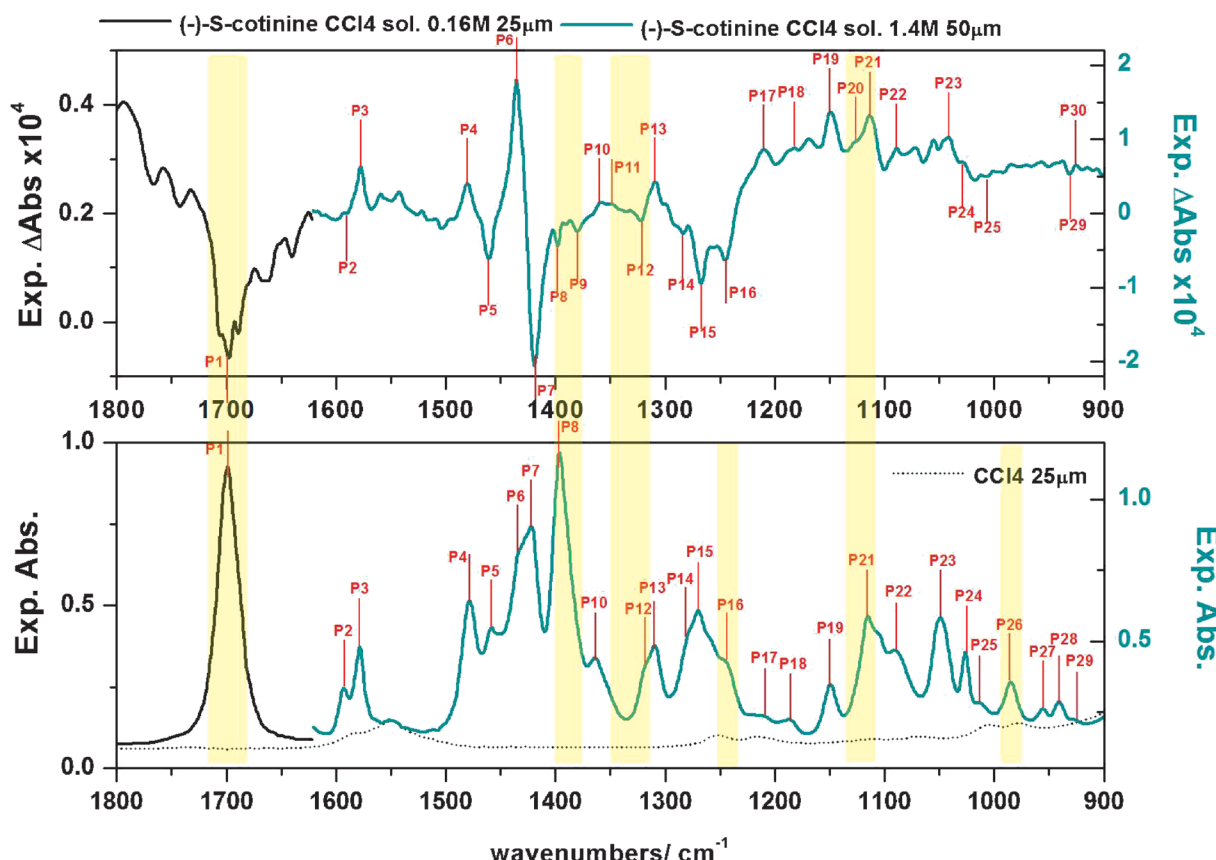


Figure 5. Recorded VCD (top) and IR (bottom) spectra of $(-)$ -S-cotinine in CCl_4 solution in the $1800\text{--}900\text{ cm}^{-1}$ region. For the recorded spectra in the $2000\text{--}1600\text{ cm}^{-1}$ region, sample solution with concentrations of 0.16 M and $25\text{ }\mu\text{m}$ of pathlength were employed (black line). The spectra obtained in the $1600\text{--}900\text{ cm}^{-1}$ region were recorded employing sample solutions 1.4 M and $50\text{ }\mu\text{m}$ (green line).

rotational strengths (R_i), and the proposed vibrational assignment.

VCD and IR experimental spectra of $(-)$ -S-cotinine in CCl_4 solution are accurately reproduced by the scaled Boltzmann-averaged theoretical spectra (B3LYP/aug-cc-pVTZ) (Figure 7). The good match between theory and experiment allows us to assign the experimental features appearing in the $1750\text{--}900\text{ cm}^{-1}$ region to the following normal modes: $\nu\text{C=O}$ of the pyrrolidinone ring, $\delta_{\text{ip}}\text{CH}$ of the pyridine ring, $\delta^{35}\text{CH}_3$ and $\delta^5\text{CH}_3$ of the $\text{N}-\text{CH}_3$ group, $\nu\text{N}-\text{CO}$, scissoring CH_2 , rocking CH_2 and $\delta\text{C}^*-\text{H}$ of the pyrrolidinone ring, νCC of the pyridine ring, wagging C=O , $\delta_{\text{ip}}\text{CCC}$ and $\delta_{\text{oop}}\text{CH}$ of the pyridine ring, as well as to the pyridine and pyrrolidinone rings breathing normal modes, in accordance with the theoretical wavenumbers calculated for the set of conformers of $(-)$ -S-cotinine (see Table 2).

As will be later discussed, the determination of the solution-state conformer population of $(-)$ -S-cotinine can be carried out taking the VCD data as reference rather than the IR data. The experimental features of interest in this regard are: P_1 , 1700 cm^{-1} (–), P_8 , 1398 cm^{-1} (–), P_9 , 1380 cm^{-1} (–), P_{11} , 1347 cm^{-1} (+), P_{12} , 1321 cm^{-1} (+), P_{20} , 1126 cm^{-1} (+) and P_{21} , 1113 cm^{-1} (+). As shown in Figures 7 and 8 and in Table 2, some of these bands can either be assigned to the normal modes of a particular molecular conformation or to the observed spectral profile (i.e., wavenumbers, band shapes and

relative intensities) in a given region of the VCD spectrum. This assignment can only be justified if all the conformers are considered to be present in the sample in a specific relative amount. Thus, the abovementioned bands (which are accurately predicted by our theoretical results) are the key to state the presence of minor conformations in addition to the global minimum.

Starting from the higher-wavenumber region, the shape and magnitude of the so-called P_1 appearing in the VCD spectrum (assigned to the C=O stretching normal mode) can be justified if all the conformers are present in a $4:2:2:1$ ratio in the sample (see Figure 8a). The corresponding vibrational wavenumbers calculated for both the main conformer **m01** and its rotational isomer **m02** are predicted to be very weak and positive ($+3.6 \times 10^{-44}$ and $+8.2 \times 10^{-44}$ esu^2cm^2 , respectively) while the observed VCD band is negative. The magnitude and sign of this experimental band can be explained by considering the contribution of **m03** and **m04** species to the VCD spectral profile of the sample, as both are predicted to show a negative peak at this wavenumber which, besides, is calculated to be rather more intense (-18.5×10^{-44} and -14.9×10^{-44} esu^2cm^2 , respectively). The counterpart of P_1 in the IR spectrum is an intense broad band whose assignment does not allow making any conformational discrimination.

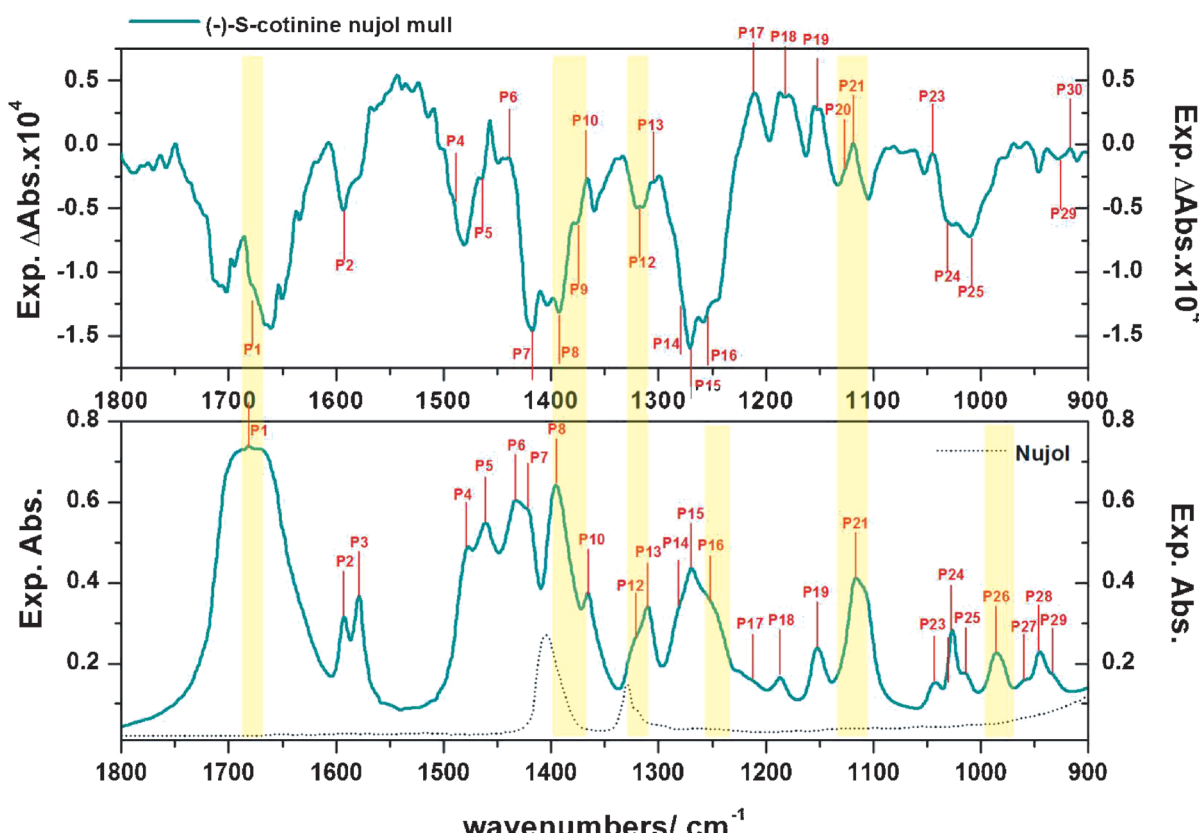


Figure 6. Recorded VCD (top) and IR (bottom) spectra of (*-*)-S-cotinine in nujol mull in the 1800–900 cm^{-1} region.

Also quite informative is the spectral feature P8 in the VCD spectrum, which can be assigned only to normal modes of conformers **m03** and **m04** (see Table 2 and Figure 8a). Although the Boltzmann-weighted IR spectrum predicts the presence of P8 in the IR spectrum as well (Figure 8b), band broadening and overlapping phenomena seem to prevent its experimental observation (Figures 7c,d). As shown in Figure 5, the IR spectrum present a broad band centered at 1396 cm^{-1} , which is clearly resolved into two negative peaks in the VCD spectrum, namely P8 and P9, the latter of which can be attributed to conformers **m01** and **m02**.

Similarly, the peaks called P10 and P11 in the VCD spectrum are not resolved in the IR spectrum, where only a broad band centered at 1365 cm^{-1} can be observed. Nonetheless, the theoretical Boltzmann-averaged VCD spectrum for a ca. 4:2:2:1 conformational mixture accurately reproduces the shape of this spectral region. These peaks are assigned to the $\delta_{\text{ip}}\text{CH}^{\text{PYR}}$ normal mode combined with the $\delta\text{C}^*-\text{H}$ normal mode of the pyridine and pyrrolidinone rings, respectively, in conformers **m01** and **m02** (P10) and to the same vibrational motion in **m03** and **m04** (P11).

The theoretical reproduction of P12 in the VCD spectrum is also possible considering an approximate 4:2:2:1 conformational population (Figure 8a). This peak is assigned to the $\delta_{\text{ip}}\text{CH}^{\text{PYR}}$ normal mode combined with the $\delta\text{C}^*-\text{H}$ and ρCH_2 normal modes of the pyridine and pyrrolidinone rings of the four conformers (Table 2). The rotational strengths calculated for the four conformers are as follows: -5×10^{-44} (**m01**), $-1 \times$

10^{-44} (**m02**), $+20 \times 10^{-44}$ (**m03**) and $+13 \times 10^{-44}$ (**m04**) esu^2cm^2 . So, the sign, position and band shape of P12 VCD feature can be understood, considering the negative contribution to the observed peak of **m01 + m02** (present in higher amounts) together with the rather more intense and positive character of these normal modes as calculated for **m03 + m04**, which would be present in lower amounts.

Finally, following the same logic, the shape of P20 (which is a subtle shoulder in the VCD and non-observable in the IR spectrum) may be justified considering the presence of the four conformers in the theoretically estimated amounts. It has been assigned to the ρCH_3 combined with the $\delta_{\text{ip}}\text{CH}^{\text{PYR}}$, in accordance with their theoretical wavenumbers (see Table 2).

Further, besides the observations in the VCD spectrum, some additional features in the IR spectrum may also point to the existence of a conformational mixture. For example, the features P16 (weak shoulder centered at 1244 cm^{-1}) and P26 (centered at 984 cm^{-1} and not identified in the VCD spectrum), can also be tentatively assigned to **m03 + m04** (Figures 8b,c).

At this point it is worth mentioning that some of the experimental VCD peaks discussed above have been assigned to non-robust vibrational modes according to the criteria reported elsewhere^[71,72] (Table S1 collects the values of the rotational strengths and the ETDM–MTDM (ξ) angles for the normal modes of (*-*)-S-cotinine in the region of interest). Nonetheless, although the arguments presented above have to be considered with a certain caution, we consider that we report enough individual pieces of evidence (using two different the-

Table 2. Wavenumbers of the observed VCD and IR bands for (–)-S-cotinine in CCl_4 solution and nujol mull, along with their theoretical correspondence and proposed assignment. The signs of the experimental VCD peaks (in brackets) and the sign and magnitude of their calculated theoretical rotational strengths (R_i) are also shown.^[a,b]

Peak	Experimental		Scaled B3LYP/augTZ PCM CCl_4								Assignment				
	IR Peak	Nujol	VCD		m01		m02		m03		m04				
			CCl ₄	Nujol	ν	R_i	ν	R_i	ν	R_i					
P1	1682	vbr	1700 sharp	1681(–)	1700(–)	1681	+4	1682	+8	1677	–18	1679	–15	$\nu\text{C}=\text{O}$	
P2	1592		1594	1592(–)	1594(–)	1581	–3	1582	+3	1579	–3	1580	+3	$\delta_{\text{ip}}\text{CH}^{\text{PYR}}$	
P3	1579		1579		1578(+)	1565	+27	1566	+24	1566	+25	1565	+25	$\delta_{\text{ip}}\text{CH}^{\text{PYR}}$	
P4	1479	br	1478 br	1481(–)	1480(+)	1471	+2	1470	+21	1473	+18	1473	+35	$\delta^{\text{as}}\text{CH}_3$	
P5	1462	br	1459 br	1465(–)	1461(–)	1456	–11	1456	–5	1458	–8	1459	–6	scCH_2	
					1448	+4	1448	+4	1447	+1	1447	+3	$\delta^{\text{as}}\text{CH}_3$		
					1427	+2	1428	+11	1432	+8	1431	–1	scCH_2		
P6	1434	sh,br	1434 sh,br	1438(+)	1435(+)	1421	+70	1423	+56	1421	+107	1424	+57	$\text{sc}\text{CH}_2 + \delta_{\text{ip}}\text{CH}^{\text{PYR}} + \delta\text{C}^*\text{-H}$	
P7	1423	vbr	1422 vbr	1417(–)	1419(–)	1404	–48	1404	–31	1405	–106	1405	–45	$\delta^{\text{s}}\text{CH}_3$	
P8	1394	br	1396 br	1403(–)	1398(–)					1381	–25	1380	–18	$\delta^{\text{s}}\text{CH}_3 + \delta\text{C}^*\text{-H} + \nu\text{N}-\text{CO}$	
P9				1375(–)	1380(–)	1367	–19	1366	–24					$\delta^{\text{s}}\text{CH}_3 + \delta\text{C}^*\text{-H} + \nu\text{N}-\text{CO}$	
P10				1367(+)	1359(+)	1353	+27	1353	+24					$\delta_{\text{ip}}\text{CH}^{\text{PYR}} + \delta\text{C}^*\text{-H}$	
P11	1365	br	1362 br	1342(+)	1347(+)					1347	+36	1346	+36	$\delta_{\text{ip}}\text{CH}^{\text{PYR}} + \delta\text{C}^*\text{-H}$	
P12	1324	sh	1318 sh	1317(–)	1321(–)	1313	–5	1316	–1	1311	+20	1314	+13	$\delta_{\text{ip}}\text{CH}^{\text{PYR}} + \delta\text{C}^*\text{-H} + \rho\text{CH}_2$	
P13	1310		1309	1307(+)	1309(+)	1297	+29	1299	+14	1301	–17	1301	–10	ρCH_2	
P14	1281	sh	1278 sh	1285(–)sh	1284(–)	1273	–36	1273	–35	1270	+61	1270	+57	ρCH_2	
P15	1268		1269	1271(–)	1268(–)	1259	–99	1258	–101	1250	–12	1247	–9	$\nu\text{CC}^{\text{PYR}} + \rho\text{CH}_2 + \delta\text{C}^*\text{-H}$	
P16	1244	sh	1244 sh	1244(–)	1244(–)	1238	–2	1239	–45	1233	–15	1233	–41	$\delta_{\text{ip}}\text{CCC}^{\text{PYR}} + \nu\text{CC}^{\text{PYR}}$	
P17	1210		1208	1210(+)	1210(+)	1206	–9	1196	+41	1206	+0.3	1199	–8	$\delta_{\text{ip}}\text{CH}^{\text{PYR}} + \delta\text{C}^*\text{-H}$	
P18	1186		1186	1181(+)	1182(+)	1195	+47	1192	+17	1191	–10	1188	+6	ρCH_2	
					1174	+9	1181	–7	1169	–5	1178	–6	$\delta_{\text{ip}}\text{CH}^{\text{PYR}}$		
P19	1153		1149	1152(+)	1149(+)	1133	+33	1134	+44	1131	+17	1131	+17	ρCH_2	
P20				1126(+sh)	1126(+sh)	1117	+2	1118	+3	1115	+10	1116	+13	$\rho\text{CH}_3 + \delta_{\text{ip}}\text{CH}^{\text{PYR}}$	
P21	1116		1116	1119(+)	1113(+)	1102	+30	1105	+42	1106	+5	1104	+9	$\delta_{\text{ip}}\text{CH}^{\text{PYR}}$	
P22				1089		1092	+22	1091	–0.5	1087	+60	1087	+27	$\rho\text{CH}_3 + \nu\text{CC}^{\text{PYR}}$	
					1034	–3	1036	+6	1036	–3	1036	–3	$\nu\text{CC}^{\text{PYR}}$		
P23	1044		1048	1044(+)	1041(+)	1028	+10	1027	+10	1025	+0.5	1025	+4	$\rho\text{CH}_2 + \text{w}\text{C}=\text{O}$	
P24	1026		1026	1028(–)	1030(–)	1012	+0.8	1012	+3	1013	–5	1012	+9	$\delta_{\text{ip}}\text{CCC}^{\text{PYR}}$	
P25	1012		1011	1010(–)	1006(–)	991	+0.7	988	–0.2	999	–3	998	–6	$\delta_{\text{oop}}\text{CH}^{\text{PYR}}$	
P26	986		984			986	+5	986	+4	990	–0.4	988	–0.04	$\nu\text{CC}^{\text{PYR}} + \rho\text{CH}_3$	
P27	959		956			966	+7	967	+4	967	+2	968	–0.5	$\delta_{\text{oop}}\text{CH}^{\text{PYR}}$	
P28	946		940			953	+5	951	–0.5	951	–0.6	954	–1	$\delta_{\text{oop}}\text{CH}^{\text{PYR}}$	
P29	930		924			930(–)	–10	931	–10	936	+5	936	–1	$\delta_{\text{oop}}\text{CH}^{\text{PYR}}$	
P30					918(+)		926(+)		921	+9	913	–5	913	+2	$\delta_{\text{oop}}\text{CH}^{\text{PYR}} + \text{breath}^{\text{PYR/pyr}}$

[a] Scaled theoretical wavenumbers calculated for conformers of (–)-S-cotinine in CCl_4 (implicit solvent IEF-PCM) at the B3LYP/aug-cc-pVTZ level (scale factor = 0.970 taken from the Computational Chemistry Comparison and Benchmark Database, Ref. [73]). Calculated rotational strengths ($R_i \times 10^{-44}$) in esu^2cm^2 are shown in brackets. All modes have A symmetry. [b] Symbols used: ν = stretching, δ = deformation, ρ = rocking, sc = scissoring, tw = twisting, w = wagging, breath = breathing, br = broad, sh = shoulder. Superscript * denote asymmetric carbon. Superscripts "s" and "as" denote symmetric and asymmetric motions of the NVM. Subscripts "ip" and "oop" denote in-plane and out-of-plane vibrational motions. The superscript PY stands for pyridine ring and the superscript pyr stands for pyrrolidinone ring. The description of the vibrational modes is proposed by means of their visual inspection using Gaussview 5.0.

oretical methods) always pointing in the same direction: the occurrence of conformational mixture and the 4:2:2:1 population distribution.

In the search of further proof for this conclusion, we estimated the averaged IR and VCD spectra of three different hypothetical sample compositions, namely: 1:1:1:1 (25 % of each conformer), 4:2:2:1 (44.4 % **m01**, 22.2 % **m02**, 22.2 % **m03**, 11.1 % **m04** which is close to the theoretical composition given by the B3LYP/aug-cc-pVTZ level in the IEF-PCM model), and 1:2:2:4 (11.1 % **m01**, 22.2 % **m02**, 22.2 % **m03**, 44.4 % **m04**). The comparison of the resulting weighted profiles with the experimental IR and VCD spectra of the sample in solution are shown in Figures S3 and S7.

Concerning the VCD spectral profile (Figure S3), the best theoretical-experimental match is achieved when the proportion of the different conformers is set to 4:2:2:1, whilst the 1:1:1:1 and 1:2:2:4 weighted spectra fail in the reproduction of the 1300–1200 cm^{-1} region, of key interest in this study. Nevertheless, the theoretical-experimental match reached for the IR spectra of the sample is comparable (and rather good) for all the conformer distributions considered (Figure S7). Further, most of the spectral features observed in the experimental IR spectra could be justified considering that a unique molecular configuration (whether **m01**, **m02**, **m03** or **m04**) is present in the sample. In contrast, the experimental VCD spectra, that tend to show a good quantity of unique conformational and

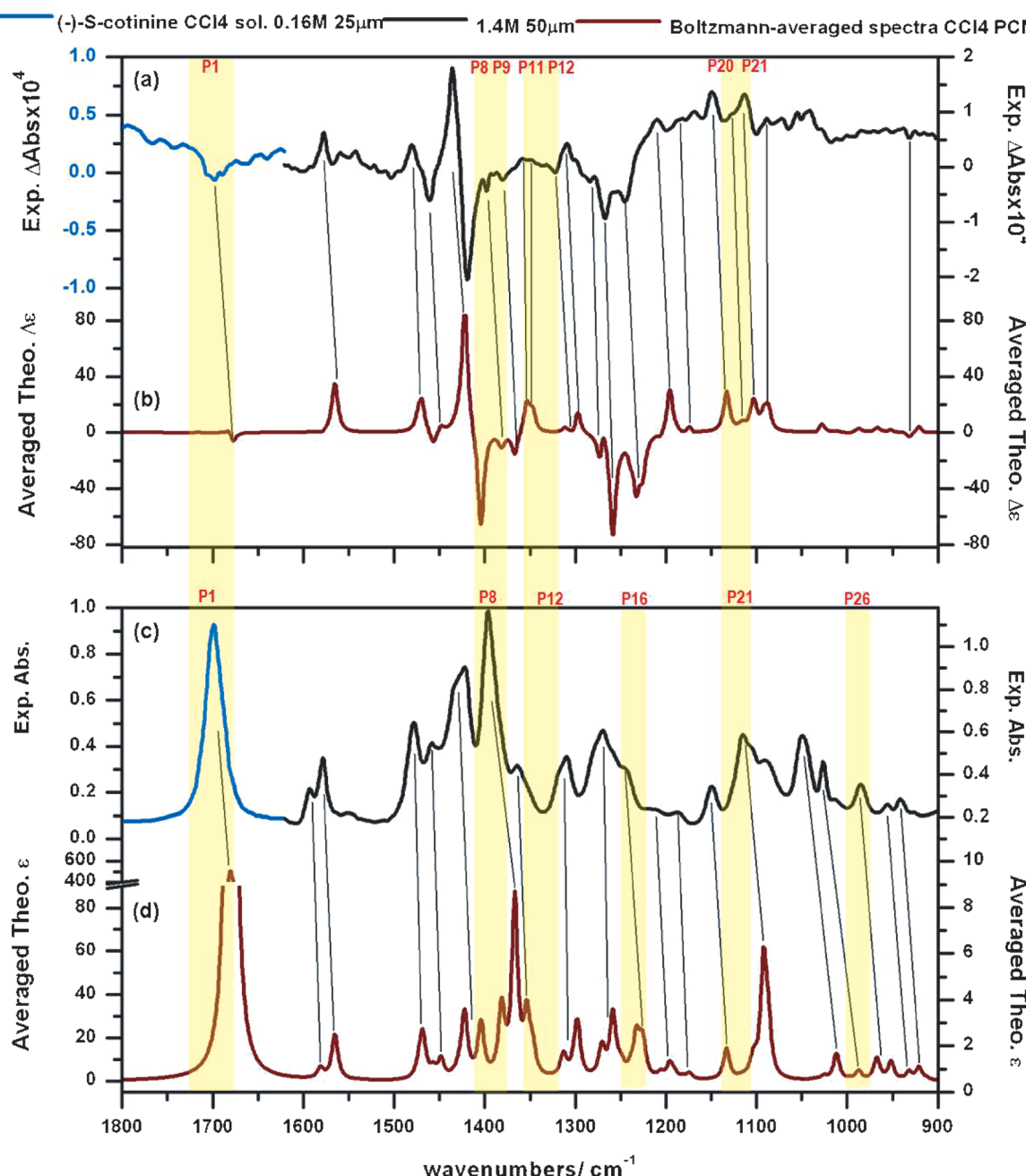


Figure 7. Experimental VCD (top) and IR (bottom) spectra of (*-*)-S-cotinine compared with the predicted scaled B3LYP/aug-cc-pVTZ Boltzmann-averaged spectra in the 1800–900 cm^{-1} region: a,c) CCl_4 solution, resolution 4 cm^{-1} , 2000 scans (blue 0.16 M, 25 μm ; black 1.4 M, 50 μm), b,d) Boltzmann-averaged spectra calculated in CCl_4 (IEF-PCM, Boltzmann's populations at 298.15 K, FWHM = 8 cm^{-1} , Scale Factor = 0.970 taken from Ref. [73]). The regions of interest for the conformational analysis are highlighted.

structural-related spectral signals in the mid-IR region, together with the different calculated VCD profiles for each conformation, aided in identifying the dominant species in solution. Thus, these results confirm the enhanced capability of VCD spectroscopy, comparing with its non-chiral-sensitive counterpart (FTIR) for solving the solution-state conformational composition of chiral samples, even in cases, such as (*-*)-S-cotinine, in which only subtle structural changes distinguish the different conformers.

3. Conclusions

The conformational landscape of (*-*)-S-cotinine was studied, employing a double strategy comprising the use of DFT (B3LYP and B3PW91) calculations and vibrational spectroscopies. Up to four subtly dissimilar molecular conformations are populated at room temperature both in the gas phase and in solution—in both cases the relative conformational population is close to 4:2:2:1 (**m01:m02:m03:m04**). The energy barrier associated with the rotational isomerism in the lower-energy

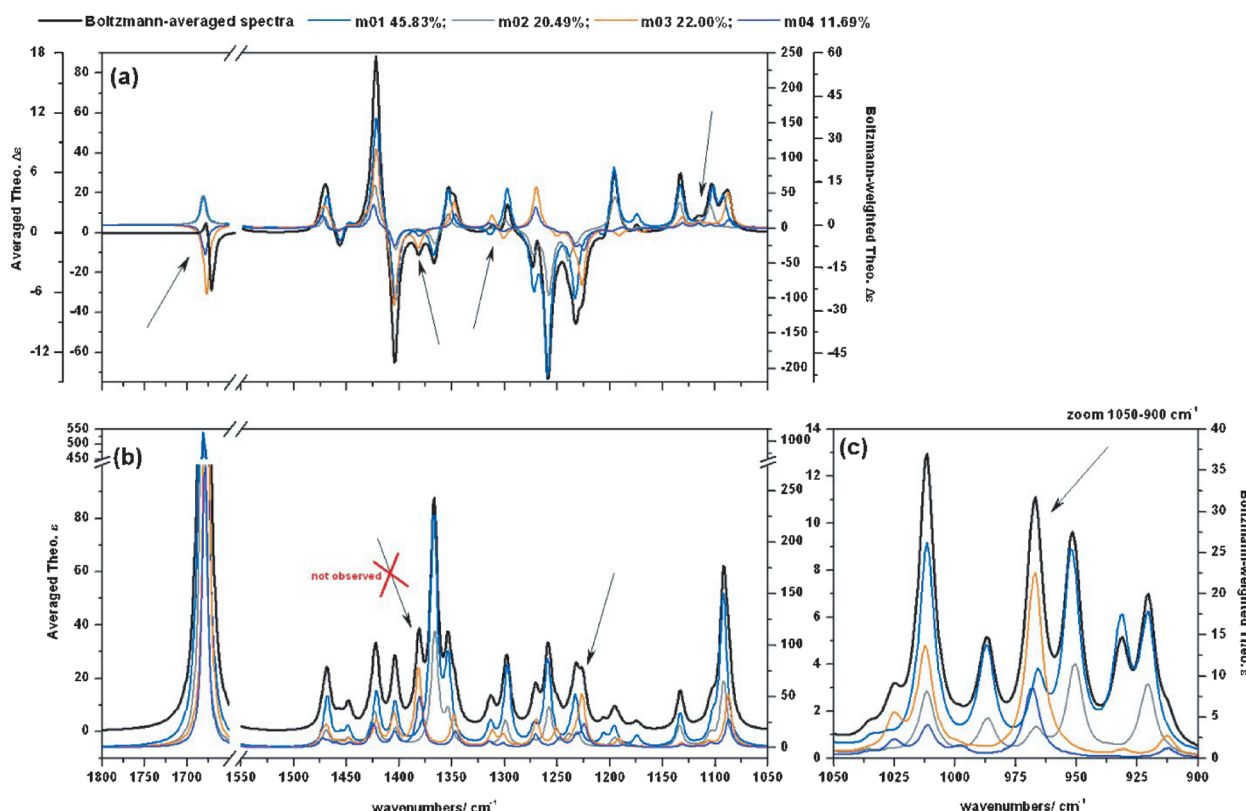


Figure 8. Predicted scaled B3LYP/aug-cc-pVTZ Boltzmann-averaged spectra calculated in CCl_4 (IEF-PCM, Boltzmann's populations at 298.15 K, FWHM = 8 cm^{-1} , Scale Factor = 0.970 taken from Ref. [73]), a) VCD 1800–1050 cm^{-1} ; b) IR 1800–1050 cm^{-1} ; c) IR 1050–900 cm^{-1} , compared with the corresponding Boltzmann-weighted spectra calculated for each conformer of (–)-S-cotinine. The features discussed within the text are marked with an arrow.

conformers (eq structures, **m01** and **m02**) was determined and analyzed by ab initio and NBO calculations, leading us to conclude that hyperconjugative delocalizations are the dominant force governing the conformational preference in this species. Calculations in solution (IEF-PCM in CCl_4 and DMSO) support this fact as solvent effects are negligible (i.e., neither the structure nor the conformational energy profile of this species is strongly affected by solvent's polarity since they barely change on going from non-polar to polar media).

The VCD spectra of (–)-S-cotinine was recorded for the first time and thoroughly analyzed (both in CCl_4 solution and the solid phase using nujol mulls). The comparison of the solution-state and solid-phase VCD data obtained may point to the occurrence of either strong packing or particle-size-related scattering effects in the solid-phase spectra. The analysis of both VCD and IR spectra was carried out employing a theoretical-experimental methodology. In this regard we address that: 1) B3LYP yields better results, resembling the experimental spectral profile recorded more than B3PW91 functional (which has been suggested to be a very good choice for computing VCD intensities^[70]); 2) the similarity between the recorded spectra in CCl_4 and the calculated spectra using the IEF-PCM approximation suggest that the continuum modeling of the solvent is a reasonably good option when using non-polar solvents for the experimental measurement.

The occurrence of the conformational mixture and the solution-state conformational population of the sample in CCl_4

have been determined by the analysis of the mid-IR region of the VCD spectra, which can only be justified by taking the relative theoretical population in CCl_4 to be ca. 45.83 % **m01**, 20.49 % **m02**, 22.0 % **m03** and 11.69 % **m04**. Confirmation for the presence of minor structures is guaranteed mainly by the experimental observation of peaks appearing in the 1400–1300 cm^{-1} region that are only attributable to **m03** and **m04** conformers and, noteworthy, not resolved in the parent IR spectrum. Thus, the added value of the VCD technique, in relation to that of FTIR, for determining solution-state conformational distribution of slightly structural constrained chiral samples has been further shown by our theoretical–experimental study of (–)-S-cotinine, which demonstrates that VCD offers unique molecular fingerprints derived from smooth skeletal motions that may not be observed in the parent IR spectrum.

Acknowledgements

The authors thank the Andalusian government for funding (FQM-173) and the Centro de Instrumentación Científico Técnico (CICT) of the University of Jaén for instrumental facilities. P. G. R. O. thanks the University of Jaén for a post-doctoral contract supporting this work (Ref. 2014/CL073 (T2-I)).

Keywords: (–)-S-cotinine • conformational landscapes • density functional calculations • molecular structures • vibrational circular dichroism

- [1] W. C. Evans, *Alkaloids in Trease and Evans 'Pharmacognosy'* 16th ed. (Ed.: P. Graham), Saunders Elsevier, Edinburgh, **2009**.
- [2] W. Bannon, M. W. Decker, M. W. Holliday, P. Curzon, D. Donnelly-Roberts, P. S. Puttfarcken, R. S. Bitner, A. Diaz, A. H. Dickenson, R. D. Porsolt, M. Williams, S. P. Arneric, *Science* **1998**, *279*, 77–81.
- [3] R. M. Elgen, J. C. Hunter, A. Dray, *Trends Pharmacol. Sci.* **1999**, *20*, 337–342.
- [4] S. N. Haydar, C. Ghiron, L. Bettinetti, H. Bothmann, T. A. Comery, J. Dunlop, S. La Rosa, I. Mico, M. Pollastrini, J. Quinn, R. Roncarati, C. Scali, M. Valacchi, M. Varrone, R. Zanaletti, *Bioorg. Med. Chem.* **2009**, *17*, 5247–5258.
- [5] H. Yuan, P. A. Petukhov, *Bioorg. Med. Chem.* **2006**, *14*, 7936–7942.
- [6] K. Calloe, R. Goodrow, S. P. Olesen, C. Antzelevitch, J. M. Cordeiro, *Am. J. Physiol. Heart Circ. Physiol.* **2013**, *305*, H66–H75.
- [7] A. Kucinski, S. Wersinger, E. K. Stachowiak, M. Radell, R. Hesse, T. Corso, M. Parry, M. Bencherif, K. Jordan, S. Letchworth, M. K. Stachowiak, *Health* **2012**, *4*, 1178–1190 (and references therein).
- [8] M. N. Tiwari, S. Agarwal, P. Bhatnagar, N. K. Singhal, S. K. Tiwari, P. Kumar, L. K. S. Chauhan, D. K. Patel, R. K. Chaturvedi, M. P. Singh, *Free Radical Biol. Med.* **2013**, *65*, 704–718M (and references therein).
- [9] M. Stornaiuolo, G. E. De Kloe, P. Rucktooa, A. Fish, R. van Elk, E. S. Edink, D. Bertrand, A. B. Smit, I. J. P. de Esch, T. K. Sixma, *Nat. Commun.* **2013**, *4*, 1875–1886.
- [10] V. Tsetlin, F. Hucho, *Curr. Opin. Pharmacol.* **2009**, *9*, 306–310.
- [11] X. Xiu, N. L. Puskar, J. A. Shanata, H. A. Lester, D. A. Dougherty, *Nature* **2009**, *458*, 534–537.
- [12] R. J. Radna, D. L. Beveridge, A. L. Bender, *J. Am. Chem. Soc.* **1973**, *95*, 3831–3842.
- [13] L. B. Kier, *Mol. Pharmacol.* **1968**, *4*, 70–76.
- [14] B. Pullman, P. Courriere, J. L. Coubeils, *Mol. Pharmacol.* **1971**, *7*, 397–405.
- [15] M. Berthelot, M. Decouzon, J. F. Gal, C. Laurence, J. Y. Le Questel, P. C. Maria, J. Tortajada, *J. Org. Chem.* **1991**, *56*, 4490–4494.
- [16] D. E. Elmore, D. A. Dougherty, *J. Org. Chem.* **2000**, *65*, 742–747.
- [17] J. Graton, M. Berthelot, J.-F. Gal, S. Girard, C. Laurence, J. Lebreton, J. Y. Le Questel, P. C. Maria, P. Naus, *J. Am. Chem. Soc.* **2002**, *124*, 10552–10562.
- [18] T. Takeshima, R. Fukumoto, T. Egawa, S. Konaka, *J. Phys. Chem. A* **2002**, *106*, 8734–8740.
- [19] M. Mora, M. E. Castro, A. Nino, F. J. Melendez, C. Muñoz-Caro, *Int. J. Quantum Chem.* **2005**, *103*, 25–33.
- [20] T. Yoshida, W. A. Farone, S. S. Xantheas, *J. Phys. Chem. B* **2014**, *118*, 8273–8285.
- [21] C. C. R. Eddy, A. Eisner, *Anal. Chem.* **1954**, *26*, 1438–1421.
- [22] E. Wada, K. Yamasaki, M. Lida, K. Saito, Y. Nakayama, *Kenkyu Hokoku Nippon Senbai Kosha Chuo Kenkyusho* **1957**, *97*, 27–39.
- [23] M. Deželić, B. Nikolin, *Spectrochim. Acta A* **1967**, *23*, 1149–1153.
- [24] M. Seydou, G. Grégoire, J. Liquier, J. Lemaire, J. P. Schermann, C. Desfrançais, *J. Am. Chem. Soc.* **2008**, *130*, 4187–4195.
- [25] M. Baranska, J. C. Dobrowolski, A. Kaczor, K. Chruszcz-Lipska, K. Gorz, A. Rygula, *J. Raman Spectrosc.* **2012**, *43*, 1065–1073.
- [26] J.-U. Grabow, S. Mata, J. L. Alonso, I. Peña, S. Blanco, J. C. López, C. Ca-bezas, *Phys. Chem. Chem. Phys.* **2011**, *13*, 21063–21069.
- [27] P. S. Hammond, Y. Wu, R. Harris, T. J. Minehardt, R. Car, J. D. Schmitt, *J. Comput. Aided Mol. Des.* **2005**, *19*, 1–15.
- [28] M. Koné, B. Illien, C. Laurence, J.-F. Gal, P.-C. María, *J. Phys. Org. Chem.* **2006**, *19*, 104–114.
- [29] J. D. Schmitt, C. G. Sharples, W. S. Caldwell, *J. Med. Chem.* **1999**, *42*, 3066–3074.
- [30] P. G. Rodríguez Ortega, M. Montejo, J. J. López González, *ChemPhysChem* **2015**, *16*, 342–352.
- [31] P. A. Crooks, M. Li, L. P. Dwoskin, *Drug Metab. Dispos.* **1997**, *25*, 47–54.
- [32] L. P. Dwoskin, L. Teng, S. T. Buxton, P. A. Crooks, *J. Pharmacol. Exp. Ther.* **1999**, *288*, 905–911.
- [33] D. Rolf, US Patent Number: 5,776,956, **1998** (and references therein).
- [34] T. Takeshima, H. Takeuchi, T. Egawa, S. Konaka, *J. Mol. Struct.* **2007**, *841*, 13–21.
- [35] V. Arnaud, J.-Y. Le Questel, M. Mathé-Allainmat, J. Lebreton, M. Berthelot, *J. Phys. Chem. A* **2004**, *108*, 10740–10748.
- [36] S. Y. Han, S. M. Hong, X. Li, *J. Colloid Interface Sci.* **2013**, *410*, 74–80.
- [37] O. Alharbi, Y. Xu, R. Goodacre, *Analyst* **2014**, *139*, 4820–4827.
- [38] T. A. Halgren, *J. Comput. Chem.* **1996**, *17*, 490–519.
- [39] T. A. Halgren, *J. Comput. Chem.* **1996**, *17*, 520–552.
- [40] T. A. Halgren, *J. Comput. Chem.* **1996**, *17*, 553–587.
- [41] T. A. Halgren, R. B. Nachbar, *J. Comput. Chem.* **1996**, *17*, 587–615.
- [42] T. A. Halgren, *J. Comput. Chem.* **1996**, *17*, 616–641.
- [43] M. Clark, R. D. Cramer, N. Van Opdenbosch, *J. Comput. Chem.* **1989**, *10*, 982–1012.
- [44] Spartan'08, Wavefunction, Inc. Irvine, CA.: Y. Shao, L. F. Molnar, Y. Jung, J. Kussmann, C. Ochsenfeld, S. T. Brown, A. T. B. Gilbert, L. V. Slipchenko, S. V. Levchenko, D. P. O'Neill, R. A. DiStasio, Jr., R. C. Lochan, T. Wang, G. J. O. Beran, N. A. Besley, J. M. Herbert, C. Y. Lin, T. Van Voorhis, S. H. Chien, A. Sodt, R. P. Steele, V. A. Rassolov, P. E. Maslen, P. P. Korambath, R. D. Adamson, B. Austin, J. Baker, E. F. C. Byrd, H. Dachselt, R. J. Doerkson, A. Dreuw, B. D. Dunietz, A. D. Dutoi, T. R. Furlani, S. R. Gwaltney, A. Heyden, S. Hirata, C.-P. Hsu, G. Kedziora, R. Z. Khalliulin, P. Klunzinger, A. M. Lee, M. S. Lee, W.-Z. Liang, I. Lotan, N. Nair, B. Peters, E. I. Proynov, P. A. Pieniazek, Y. M. Rhee, J. Ritchie, E. Rosta, C. D. Sherrill, A. C. Simmonett, J. E. Subotnik, H. L. Woodcock III, W. Zhang, A. T. Bell, A. K. Chakraborty, D. M. Chipman, F. J. Keil, A. Warshel, W. J. Hehre, H. F. Schaefer III, J. Kong, A. I. Krylov, P. M. W. Gill, M. Head-Gordon *Phys. Chem. Chem. Phys.* **2006**, *8*, 3172–3191.
- [45] M. J. Frisch, G. W. Trucks, H. B. Schlegel, G. E. Scuseria, M. A. Robb, J. R. Cheeseman, G. Scalmani, V. Barone, B. Mennucci, G. A. Petersson, H. Nakatsuji, M. Caricato, X. Li, H. P. Hratchian, A. F. Izmaylov, J. Bloino, G. Zheng, J. L. Sonnenberg, M. Hada, M. Ehara, K. Toyota, R. Fukuda, J. Hassegawa, M. Ishida, T. Nakajima, Y. Honda, O. Kitao, H. Nakai, T. Vreven, J. A. Montgomery, Jr., J. E. Peralta, F. Ogliaro, M. Bearpark, J. J. Heyd, E. Brothers, K. N. Kudin, V. N. Staroverov, R. Kobayashi, J. Normand, K. Ravaghavachari, A. Rendell, J. C. Burant, S. S. Iyengar, J. Tomasi, M. Cossi, N. Rega, J. M. Millam, M. Klene, J. E. Knox, J. B. Cross, V. Bakken, C. Adamo, J. Jaramillo, R. Gomperts, R. E. Stratmann, O. Yazyev, A. J. Austin, R. Cammi, C. Pomelli, J. W. Ochterski, R. L. Martin, K. Morokuma, V. G. Zakrzewski, G. A. Voth, P. Salvador, J. J. Dannenberg, S. Dapprich, A. D. Daniels, Ö. Farkas, J. B. Foresman, J. V. Ortiz, J. Cioslowski, D. J. Fox, *Gaussian 09, Revision D.01*, Gaussian, Wallingford, CT, USA, **2013**.
- [46] A. D. Becke, *J. Chem. Phys.* **1993**, *98*, 5648–5652.
- [47] C. Lee, W. Yang, R. G. Parr, *Phys. Rev. B* **1988**, *37*, 785–789.
- [48] J. P. Perdew, J. A. Chevary, S. H. Vosko, K. A. Jackson, M. R. Pederson, D. J. Singh, C. Fiolhais, *Phys. Rev. B* **1992**, *46*, 6671–6687.
- [49] J. P. Perdew, K. Burke, Y. Wang, *Phys. Rev. B* **1996**, *54*, 16533–16539.
- [50] J. F. Dobson, M. P. Vignale Das, *Electronic Density Functional Theory: Recent Progress and New Directions*, Springer US, Plenum, New York, **1998**.
- [51] A. D. McLean, G. S. Chandler, *J. Chem. Phys.* **1980**, *72*, 5639–5648.
- [52] R. A. Kendall, T. H. Dunning Jr., R. J. Harrison, *J. Chem. Phys.* **1992**, *96*, 6796–6806.
- [53] J. S. Binkley, J. A. Pople, *Int. J. Quantum Chem.* **1975**, *9*, 229–236.
- [54] G. A. Petersson, A. Bennett, T. G. Tensfeldt, M. A. Al-Laham, W. A. Shirley, J. Mantzaris, *J. Chem. Phys.* **1988**, *89*, 2193–2218.
- [55] G. A. Petersson, M. A. Al-Laham, *J. Chem. Phys.* **1991**, *94*, 6081–6101.
- [56] S. Miertus, E. Scrocco, J. Tomasi, *J. Chem. Phys.* **1981**, *55*, 117–129.
- [57] J. Tomasi, B. Mennucci, R. Cammi, *Chem. Rev.* **2005**, *105*, 2999–3093.
- [58] B. Mennucci, E. Cancès, J. Tomasi, *J. Phys. Chem. B* **1997**, *101*, 10506–10517.
- [59] E. Cancès, B. Mennucci, J. Tomasi, *J. Chem. Phys.* **1997**, *107*, 3032–3041.
- [60] E. Cancès, B. Mennucci, *J. Math. Chem.* **1998**, *23*, 309–326.
- [61] A. E. Reed, L. A. Curtiss, F. Weinhold, *Chem. Rev.* **1988**, *88*, 899–926.
- [62] E. D. Glendening, J. K. Badenhoop, A. E. Reed, J. E. Carpenter, J. A. Bohmann, C. M. Morales, C. R. Landis, F. Weinhold, *NBO v.6.0*. program, Theoretical Chemistry Institute, University of Wisconsin, Madison, WI, USA, **2013**.
- [63] L. A. Nafie, *Vibrational Optical Activity: Principles and Applications (Chapter 8: Measurement of Vibrational Optical Activity)*, Wiley, New York, **2011**, pp. 233–259.

- [64] a) R. Kuroda, T. Harada, Y. Shindo, *Rev. Sci. Instrum.* **2001**, *72*, 3802–32810; b) C. Merten, T. Kowalik, A. Hartwig, *Appl. Spectrosc.* **2008**, *62*, 901–905; c) T. Buffeteau, F. Lagugn-Labarthe, C. Sourisseau, *Appl. Spectrosc.* **2005**, *59*, 732–745.
- [65] P. J. Stephens, F. J. Devlin, J. R. Cheeseman, *VCD Spectroscopy for Organic Chemists (Chapter 2: The Experimental Measurement of Vibrational Absorption and Vibrational Circular Dichroism Spectra)*, CRC Press, Boca Raton, **2012**, pp. 13–46.
- [66] T. Kuppens, Ph.D. Thesis, University of Ghent (Belgium), **2006**.
- [67] A. Lesarri, E. J. Cocinero, L. Evangelisti, R. D. Suenram, W. Caminati, J.-U. Grabow, *Chem. Eur. J.* **2010**, *16*, 10214–10219.
- [68] a) E. Debie, P. Bultinck, W. Herrebout, B. van der Veken, *Phys. Chem. Chem. Phys.* **2008**, *10*, 3498–3508 (and references therein); b) V. P. Nicu, M. Heshmat, E. Jan Baerends, *Phys. Chem. Chem. Phys.* **2011**, *13*, 8811–8825 (and references therein); c) M. R. Poopari, Z. Dezhahang, Y. Xu, *Phys. Chem. Chem. Phys.* **2013**, *15*, 1655–1665.
- [69] G. Laufer, J. T. Huenke, B. S. H. Royce, Y. C. Teng, *Appl. Phys. Lett.* **1980**, *37*, 517–519.
- [70] P. J. Stephens, F. J. Devlin, J. R. Cheeseman, *VCD Spectroscopy for Organic Chemists (Chapter 4: ab initio Methods and Chapter 5: Analyses of the IR and VCD Spectra of Conformationally Rigid Molecules)*, CRC Press, Boca Raton, FL, **2012**, pp. 59–76
- [71] V. P. Nicu, E. J. Baerends, *Phys. Chem. Chem. Phys.* **2009**, *11*, 6107–6118.
- [72] V. P. Nicu, E. Debie, W. Herrebout, B. Van der Veken, P. Bultinck, E. J. Baerends, *Chirality* **2009**, *21*, E287–E297.
- [73] NIST Computational Chemistry Comparison and Benchmark Database, NIST standard reference Database 101, release 16 august **2013**, Editor: R. D. Johnson III. <http://cccbdb.nist.gov/>.

Received: January 7, 2015

Published online on March 20, 2015
